N O T I C E

THIS DOCUMENT HAS BEEN REPRODUCED FROM MICROFICHE. ALTHOUGH IT IS RECOGNIZED THAT CERTAIN PORTIONS ARE ILLEGIBLE, IT IS BEING RELEASED IN THE INTEREST OF MAKING AVAILABLE AS MUCH INFORMATION AS POSSIBLE

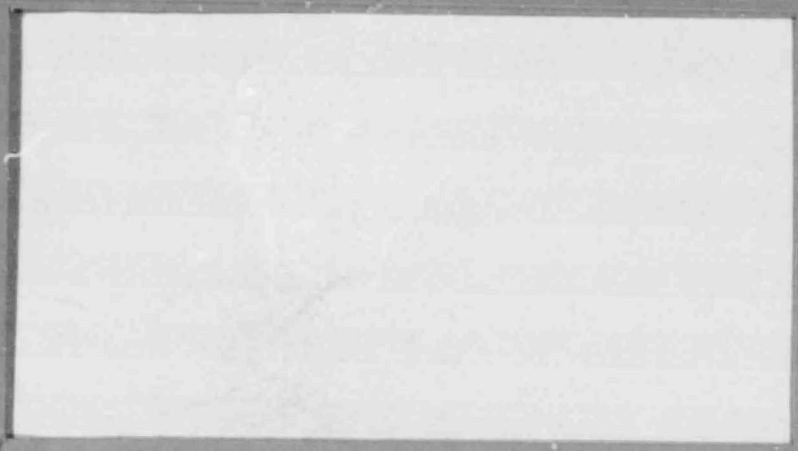

SSL

SPACE SYSTEMS LABORATORY
DEPT. OF AERONAUTICS AND ASTRONAUTICS
MASSACHUSETTS INSTITUTE OF TECHNOLOGY
CAMBRIDGE, MA 02139

DYNAMIC PROFILE OF A PROTOTYPE

PIVOTED PROOF-MASS ACTUATOR

David W. Miller

August 1981 SSL# 29-81

(Under NASA Grant #NAG1-126)

ABSTRACT

This report is intended as a documented dynamic profile of the Prototype Pivoted Proof-Mass Actuator described in the NASA contractor report, "Low-Authority Control Synthesis for Large Space Structures"; by J. N. Aubrun and G. Margulies of Lockheed Palo Alto Research Laboratory. The purpose of the work is to allow accurate compensation, for the actuator dynamics, in structural control networks used for modal excitation or suppression.

The pivoted proof-mass actuator (damper) analyzed is a prototype of a linear inertial reaction actuation device employing a flexure-pivoted reaction (proof) mass. The mass is driven by an electromechanic motor using a DC electromagnetic field and an AC electromagnetic drive. During the damping process, the actuator dissipates structural kinetic energy as heat through electromagnetic damping.

A model of the inertial, stiffness and damping properties is presented along with the characteristic differential equations describing the coupled response of the actuator and structure. The equations, employing the dynamic coefficients, are then oriented in the form of a feedback control network in which distributed sensors are used to dictate actuator response leading to a specified amount of structural excitation or damping. The scaling laws, detailed in the report mentioned above, combined with this dynamic profile yield possible actuator designs for large space structures.

ILLUSTRATIONS

Figure		Page
1	Prototype Pivoted Proof-Mass (PPM) Actuator	1
2	Terminal Locations on Prototype PPM Actuator	2
3	PPM Actuator Schematic	4
4	PPM Actuator Dynamics Model	5
5	PPM Actuator Test Setup	7
6	Phase vs. Frequency for Phase Between Driving Signal and Arm Response	9
7	Arm Deflection vs. Frequency at Constant Driving Force	10
8	Peak Arm Deflection vs. Resonant Frequency for a Particular Proof-Mass and Location	11
9	Damping Value vs. Frequency	14
10	PPM Actuator Operational Dynamics Model	16
11	PPM Actuator Operational Force Diagrams	17
a.	Pivoting Arm and Proof-Mass of Total Mass m	
b.	Nonpivoting Mount of Mass m_2	
12	Velocity Sensor Calibration vs. Deflection Amplitude	21

TABLES

Table		Page
1	Actuator Terminal Specifications	3
2	Prototype PPM Actuator Specifications	19

TABLE OF CONTENTS

	Page
OVERVIEW OF PROTOTYPE ACTUATOR	1
PPM ACTUATOR ANALYSIS	4
Test Assumptions	4
Analytical Dynamic Model	4
Test Procedure	6
Nonlinear Stiffness Property	8
Inertial Property	11
Linear Damping Model	12
INTEGRATION OF ANALYTICAL RESULTS AND OPERATIONAL DYNAMICS	15
Operational Dynamic Model	15
Stiffness and Damping Approximations	18
ADDITIONAL ACTUATOR PROPERTIES	19
Specifications	19
Motor and Velocity Sensor Calibrations	20
CONCLUSIONS AND RECOMMENDATIONS	22
REFERENCES	24

OVERVIEW OF PROTOTYPE ACTUATOR

This report provides a dynamic profile of an inertial reaction actuator for the purpose of creating effective control of a structure through the use of distributed sensors and actuators. The actuator analyzed is a prototype Pivoted Proof-Mass (PPM) Actuator developed at the Lockheed Palo Alto Research Laboratory (Fig. 1). By presenting a model of the stiffness, inertial and damping characteristics of the PPM actuator, control compensation can be developed to provide proper actuator response leading to optimal active control of a free-free structure.

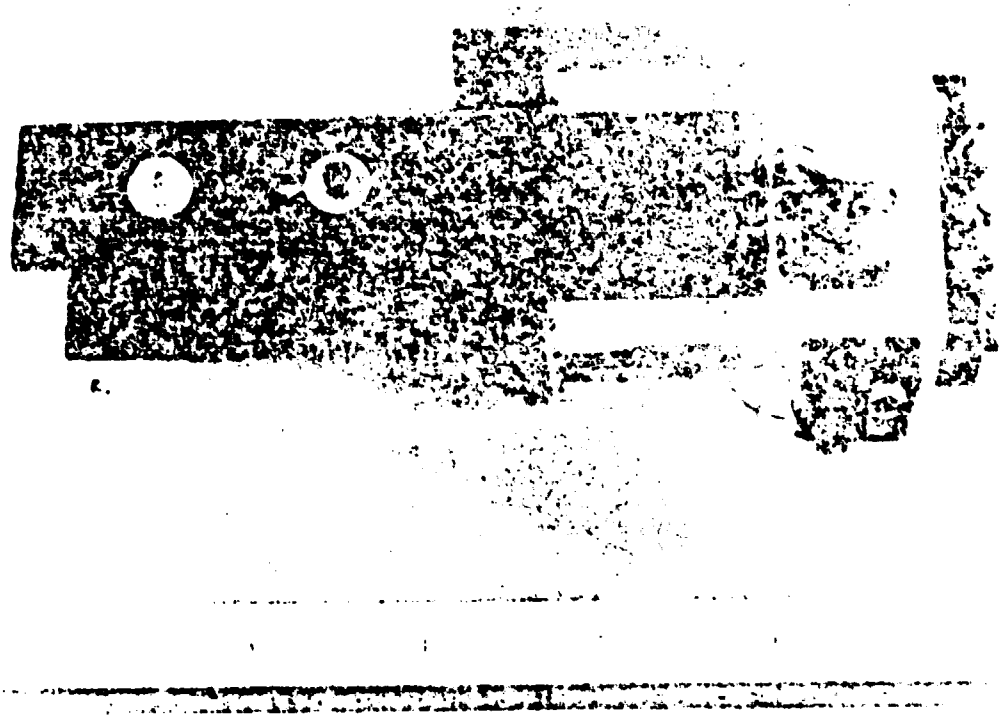

FIG. 1: Prototype Pivoted Proof-Mass (PPM) Actuator

The PPM actuator is an inertial reaction actuator which exerts a force on a structure, to which it is attached, by accelerating a separate mass element mounted on its pivoting arm. The device is effective for controlling structural

vibrations. The range of vibrational frequencies effectively controlled is determined by positioning the reaction (proof) mass, as described in Reference 1.

The PPM actuator is driven by two electromagnets: one on the pivoting arm and one on the stationary base. By eliminating the heavy magnet used in conventional linear shakers, the mass and size of the actuator is greatly reduced. Fig. 2 shows the positions of the terminals on the PPM actuator and Table 1 lists the type and electrical characteristics of each. Throughout the analysis presented in this report, the DC polarization voltage was kept at a constant 2.5 VDC. Note, in Table 1, that the power level during transient response may be allowed to exceed the limit placed on continuous steady-state operation. During actuator use, modal excitation is a steady-state operation while damping is considered a transient response.

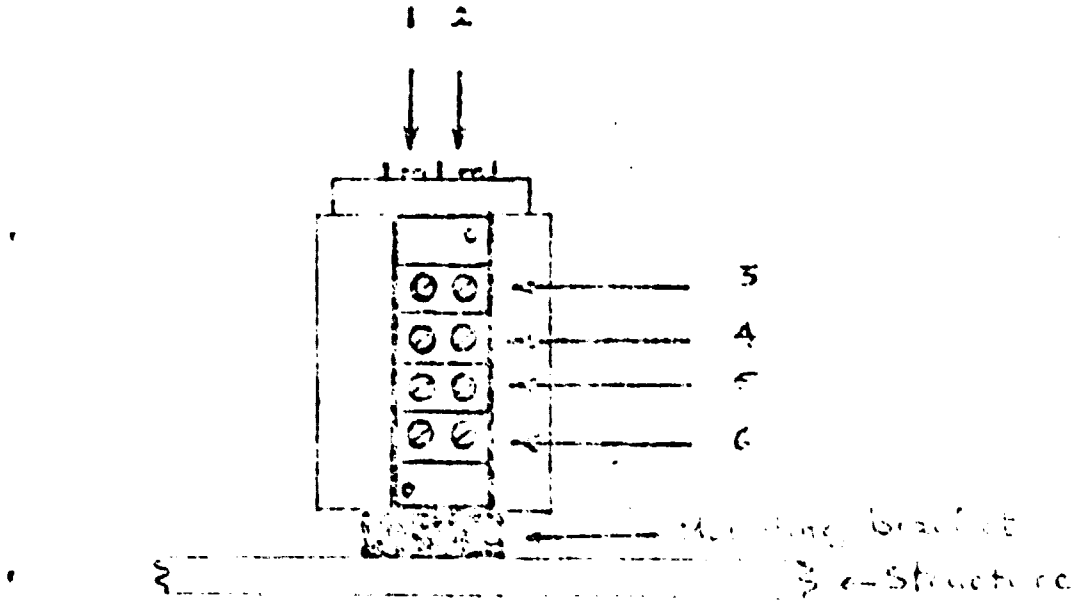

FIG. 2: Terminal Locations on Prototype PPM Actuator

TABLE 1: Actuator Terminal Specifications

Terminal #	Type	Specification
1,2	Velocity Sensor Output	See section on callibrations or Table 2.
3,4	AC Command Input During; Transient Operation	2.19 ohms ± 5.00 amps max
	Steady-State Operation	2.19 ohms ± 1.70 amps max
5,6	DC Polarization Input	1.80 ohms ± 1.20 amps max

PPM ACTUATOR ANALYSIS

TEST ASSUMPTIONS

Three basic assumptions were made at the beginning of the test procedure. The actuator was assumed to behave as a linear driven, damped system whose stiffness and damping mechanisms are located at the pivot point of the actuator arm. Since the arm pivots on a flexure, shown in Fig. 3, the stiffness assumption is valid. The damping mechanism is assumed to act at the pivot point to simplify the solution of the linear dynamic model. The feasibility of treating the actuator as a linear system will be dealt with in later sections. The linear model is derived from the force schematic in Fig. 4.

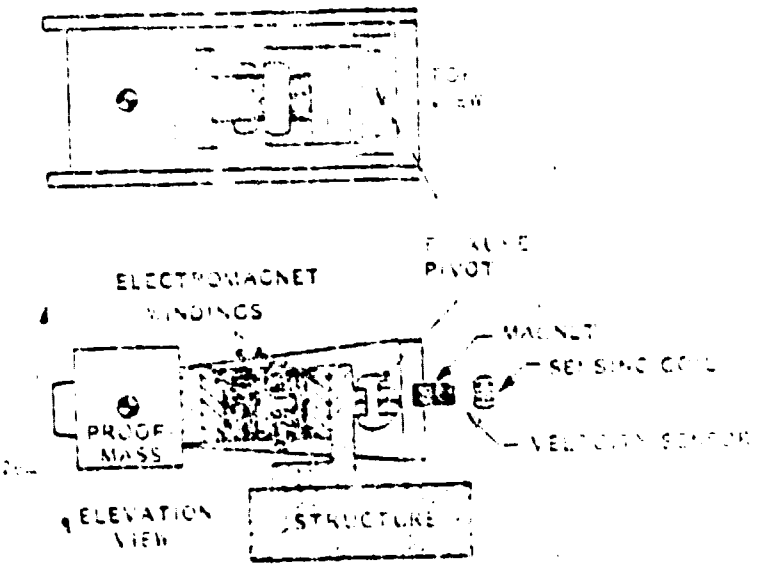

FIG. 3: PPM Actuator Schematic

ANALYTICAL DYNAMIC MODEL

The differential equation describing the motion illustrated in Fig. 4 is shown in Eq. 1. By summing the pivot arm torques, about the pivot point, the

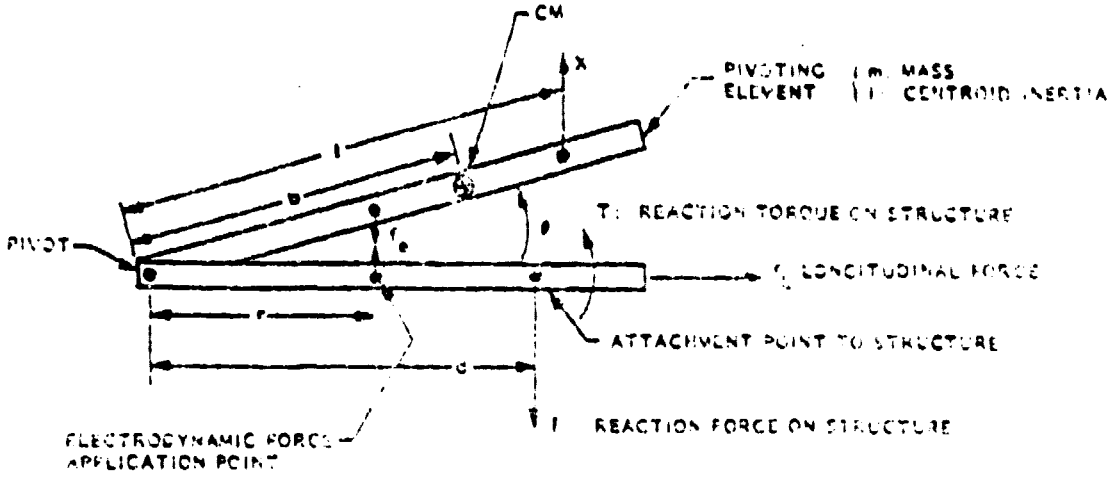

FIG. 4: PPM Actuator Dynamics Model .

equation of a damped, driven oscillator is derived.

$$[I+mb^2]\ddot{\theta} + \beta\dot{\theta} + K\theta = f_e r \qquad (1)$$

By assuming a driving force in the form,

$$f_e = f_{ea}\cos(\omega t + \phi_1) \qquad (2)$$

and a response

$$\theta = Ae^{i\omega t} \qquad (3)$$

one obtains the solution

$$\theta = \frac{f_{ea} r}{((K - \omega^2[I+mb^2])^2 + (\beta\omega)^2)^{1/2}}\cos\omega t \qquad (4)$$

where

$$\phi_1 = \tan^{-1} \frac{\beta\omega}{K - \omega^2[I+mb^2]} \qquad (5)$$

$[I + mb^2]$ is the moment of inertia of the arm and proof-mass about the pivot point and b is the location of the center of mass relative to the pivot point.

Through various tests, described in the next section, one can find the stiffness (K), inertia $[I + mb^2]$ and damping (β)values corresponding to this linear model.

TEST PROCEDURE

To obtain values of the three response coefficients, the actuator test was setup as shown in Fig. 5. The actuator was mounted to a test bed allowing the pivoting arm to swing in a horizontal plane thus minimizing gravitational effects. A proximeter was placed on one side of the reaction mass (proof-mass) to record displacement, and a load cell was positioned on the opposite side for use in calibrating the flexure stiffness.

A force-displacement curve can be made by placing shims of known thickness between the load cell and proof-mass. The resulting "zero frequency" stiffness value can be verified by calibrating the electromagnetic motor (Force/Volt) and varying the input voltage to create a force vs. deflection curve using the proximeter. The calibration of the motor is given in Table 2.

The inertia of the pivoting arm, about the pivot point, is found by recording the resonant frequency of the arm. Eq. 6 describes the resonant frequency-stiffness-inertia relation.

$$I_t = K/\omega^2 \qquad (6)$$

Since the arm is a continuous medium and the proof-mass can be considered a

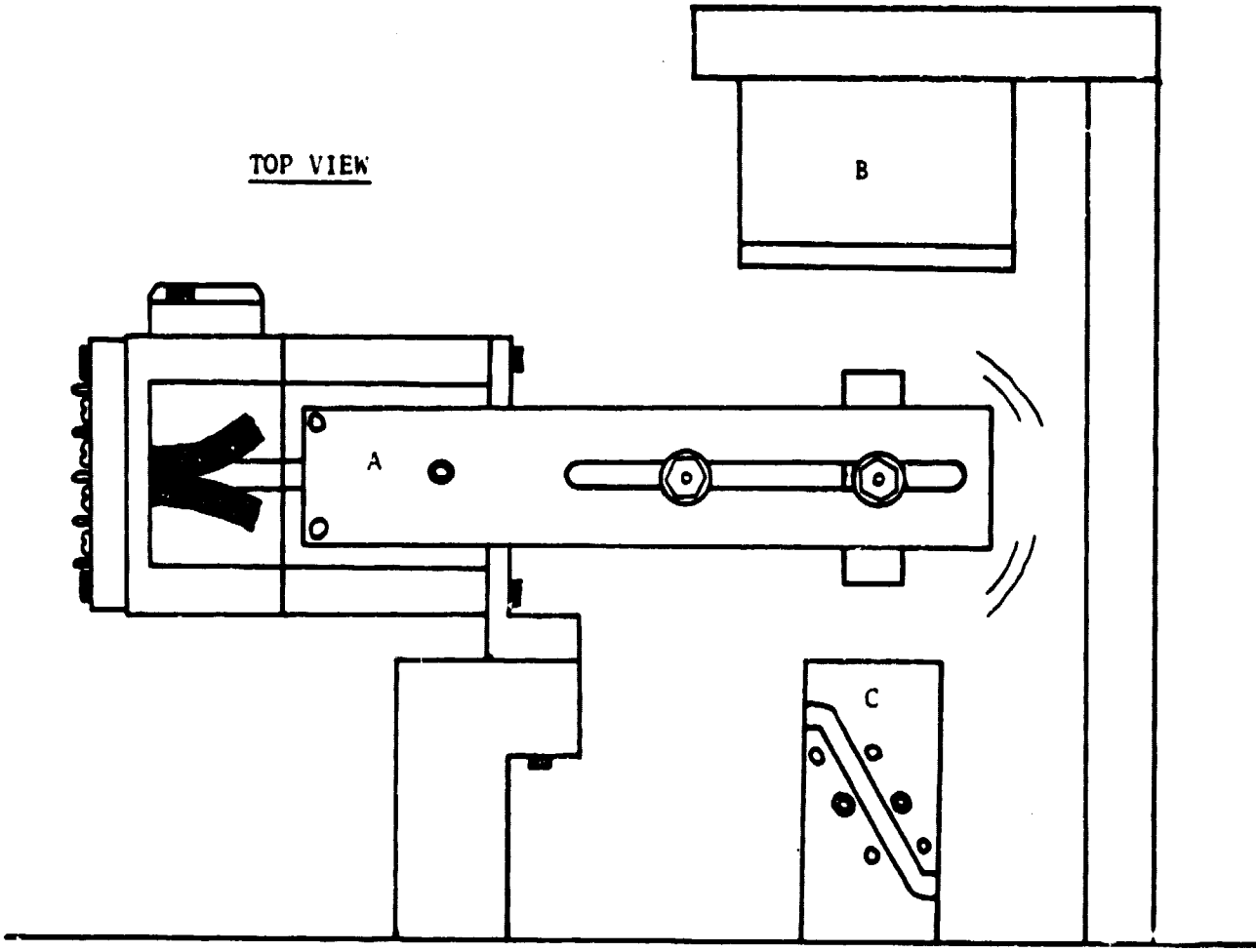

FIG. 5: PPM Actuator Test Setup
A. PPM Actuator
B. Proximeter
C. Load Cell

point mass at some distance ℓ from the pivot point,

$$I_t = I_o + m_1 \ell^2 = I + mb^2 \qquad (7)$$

where I_o is the inertia of the arm, without the proof-mass, about the pivot point. The resonant frequency can be read from the proximeter signal while the arm is undergoing free decay or being driven.

Finally, the amplitude of the motion in Eq. 4 is used to find β by record-

ing A (with the proximeter), f_{ea}, ω and using the known values of K, $[I + mb^2]$ and (r), the distance of the driving force from the pivot point.

The steps just listed were the basic steps followed in the analysis of the PPM actuator. In addition, various other tests were performed and their results either verified the results of the above tests or indicated the impracticality of that approach. Therefore, the procedure listed above was the most effective means of arriving at consistent and reliable data.

NONLINEAR STIFFNESS PROPERTY

Early in the test procedure it was evident that the PPM actuator is a nonlinear device. Fig. 6 shows a phase angle-versus-frequency plot for the phase between the input signal and the arm deflection (Eq. 5). In the plot, the data disperses as amplitude increases around resonance. The dependence of resonant frequency on amplitude indicates the presence of a variable stiffness

The occurance of the jump phenomenon on the left side of the resonant peak at 5.91 Hz. (Fig. 7) indicates that the PPM actuator has a softening nonlinearity. As the amplitude of the motion increases, decreasing pivot arm stiffness causes the resonant frequency to drop. As increased amplitude carries the electromagnets further apart during each cycle, the drop in stiffness reveals that part of the arm stiffness is contributed electromagnetically. This result was supported by amplitude dependent frequency shifts in free decay tests performed under varying polarization voltages. In addition, the location of the pivot point may shift with amplitude.

Fig. 8 is a plot of amplitude versus resonant frequency. This graph verifies the existence of a softening spring. Eq. 8 represents the resonant

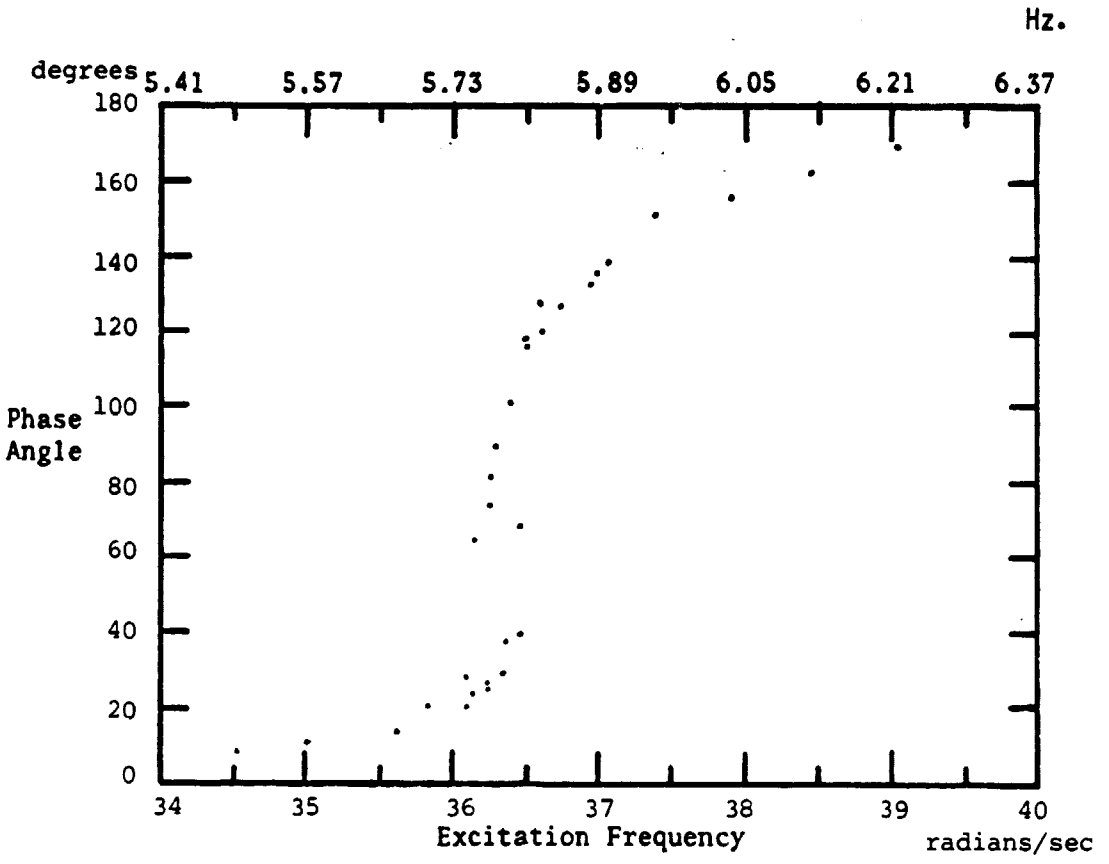

FIG. 6: Phase vs. Frequency Curve for Phase Between Driving Signal and Arm Response

frequency's amplitude dependence where ω_1 is the resonant frequency at a given amplitude A (radians) and ω_n is the resonant frequency approached as amplitude tends towards zero. ω_n varies, according to Eq. 9, as the position and mass of the proof-mass is altered.

$$\omega_1^2 = \omega_n^2 - 563A^{0.65} \tag{8}$$

$$\omega_n^2 = \frac{K_o}{I_o + m_1 \ell^2} \quad ; \quad K_o = 0.4506 \text{ N-m} \tag{9}$$

K_o is the zero-amplitude stiffness of the pivoting arm. This value is independent of the position of the proof-mass, and is the value of K found

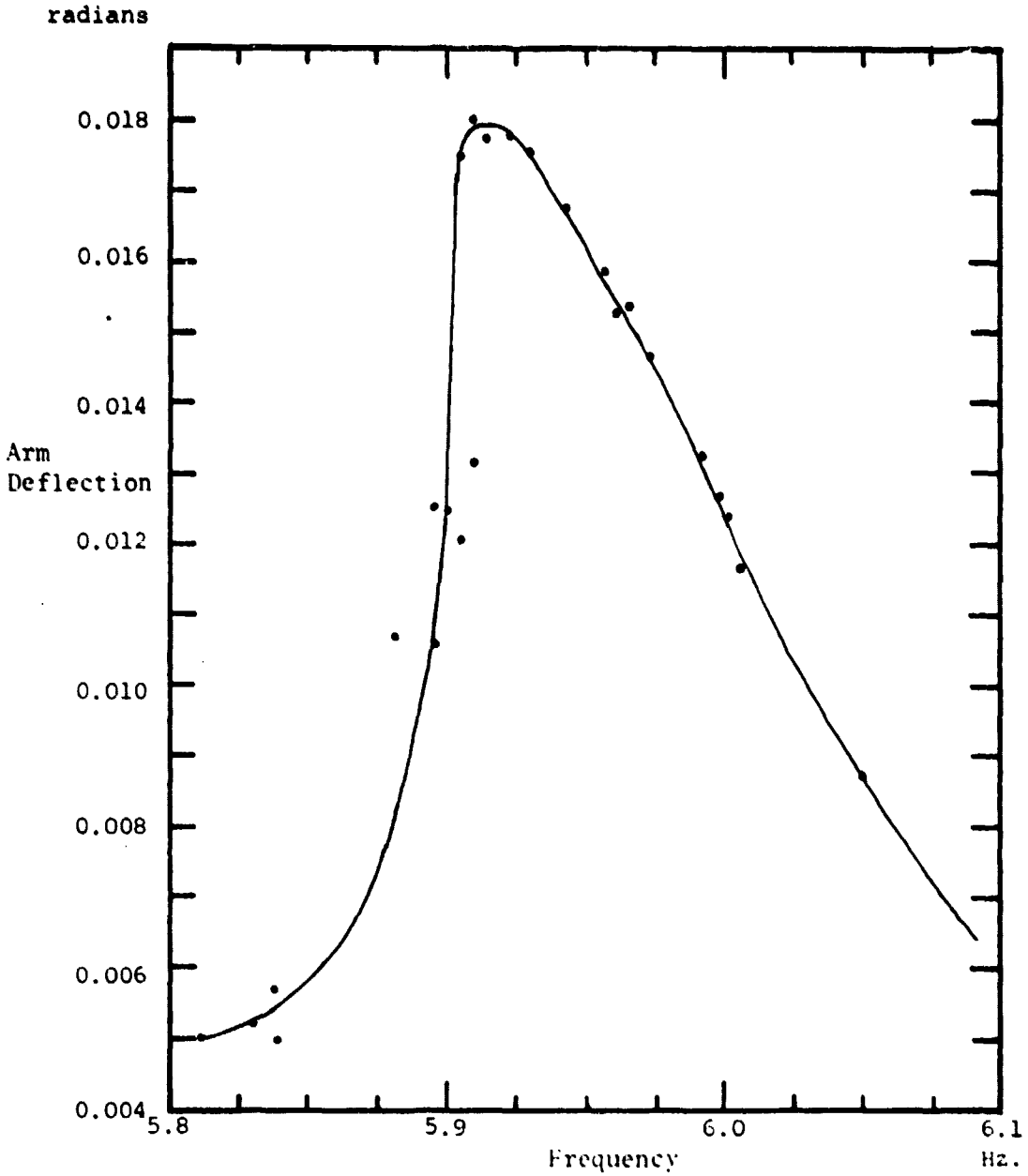

FIG. 7: Arm Deflection vs. Frequency at Constant Driving Force

during the static test. The stiffness of the arm, corresponding to a given deflection amplitude and proof-mass position, is given in Eqs. 10a and b.

$$K = \omega_1^2 [I_0 + m_1 \ell^2] \tag{10a}$$

$$= K_0 - 563 [I_0 + m_1 \ell^2] A^{0.65} \tag{10b}$$

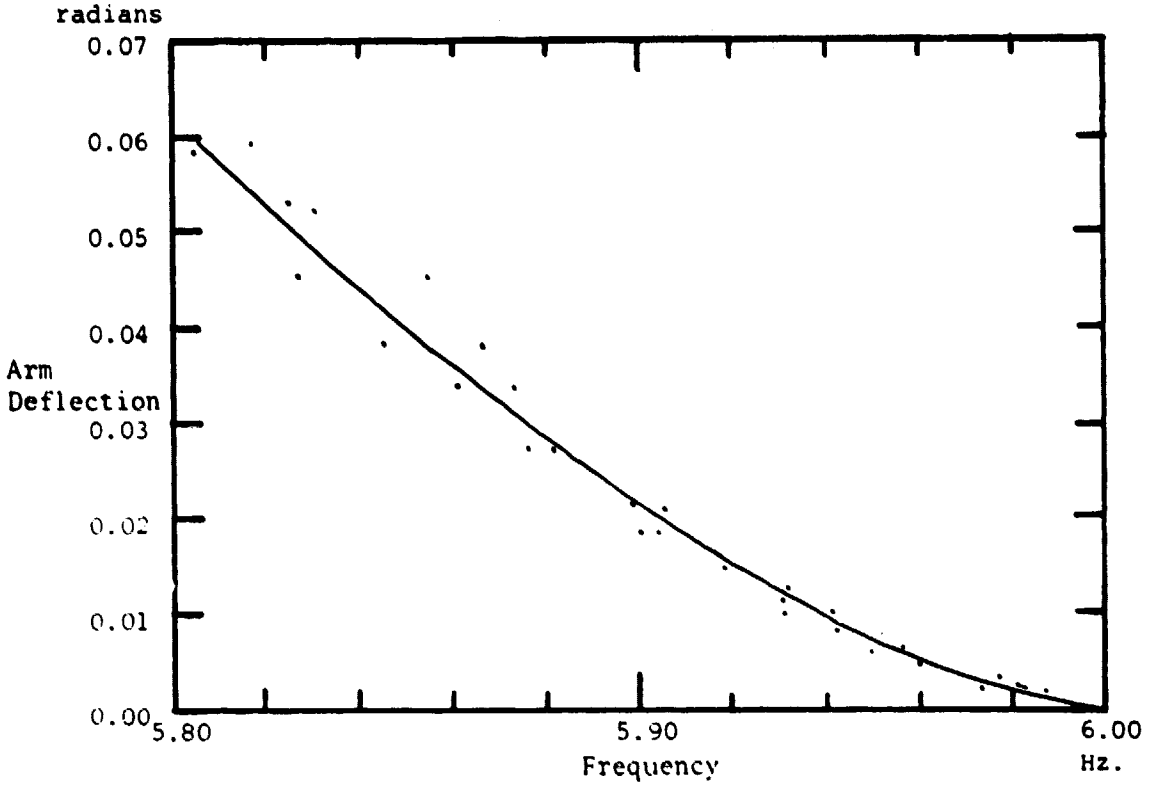

FIG. 8: Peak Arm Deflection vs. Resonant Frequency for a Particular Proof-Mass and Location (m_1=.0836 kg, l=.0545m)

INERTIAL PROPERTY

The inertia of the arm and proof-mass about the pivot point can be found using the data already retrieved. From Fig. 8 at zero amplitude, Eqs. 10a and 10b become,

$$K = \omega_n^2[I_o+m_1 \ell^2] \tag{11a}$$

$$K = K_o \tag{11b}$$

combining these results and subtracting off the proof-mass term ($m_1 \ell^2$), the inertia of the arm without the proof-mass is I_o=6.88 x10^{-5} kgm^2. Since m_1 and

ℓ may be altered, a model of the damping is all that is required to complete the solution.

LINEAR DAMPING MODEL

Fig. 9 shows the damping term, derived through Eq. 4, versus frequency for a particular proof-mass and position. The lack of data points near resonance obscures the "softening spring" effect. By recording the amplitude of the signal into the motor, converting from voltage to force (f_{ea}) and noting the frequency and resulting amplitude, the stiffness and inertial terms can be used to find the representative damping value. Each curve is at constant amplitude thus leaving frequency and driving force variable. The minimum point on the damping value curve will shift position according to the value of ω_n. The damping plot, closely resembling the driving force curve, indicates that electromagnetic damping dominates the damping process.

Since f_e is the desired result from the control loop, β must be curve fit as a function of amplitude and frequency. In other words, by rearranging the amplitude from Eq. 4, the mathematical f_e dependancy of β must be eliminated (Eq. 12).

$$\beta = ((f_{ea} r/A\omega)^2 - ((K - \omega^2[I+mb^2])/\omega)^2)^{1/2} = f(A, \omega) \qquad (12)$$

Referring to Fig. 9, Eqs. 13a and b represent the characteristic linear damping terms for frequencies less than and greater than ω_n, respectively. Deflection amplitude in radians and frequency in radians per second yields damping values in newton-meter-seconds.

$$\beta = [(A)^{2.03} + .0034][(-.195A^{0.52} + .0933)[\omega_n - \omega]^{(45A^2 + 1.245)} + .0672] \text{ N-m-sec} \qquad (13a)$$

$$\beta = [(A)^{2.03} + .0034][0.0849[\omega - \omega_n]^{1.0437} + .0672] \text{N-m-sec} \qquad (13b)$$

These equations provide a continuous representation of the damping as defined by Eq. 12. This model has been determined to be accurate in a bandwidth 8 Hz. centered at resonance. The model should be effective over a much wider range of frequencies.

It should be emphasized that this damping relation is only a representation of the PPM actuator's true damping characteristics. In Eq. 1, β is defined solely as a velocity dependent mechanism. It is later shown to be dependent on various other parameters. Consequently, the sole purpose of this approach is to provide a dynamic model which can be used in a control system to determine actuator inputs which will produce desired outputs.

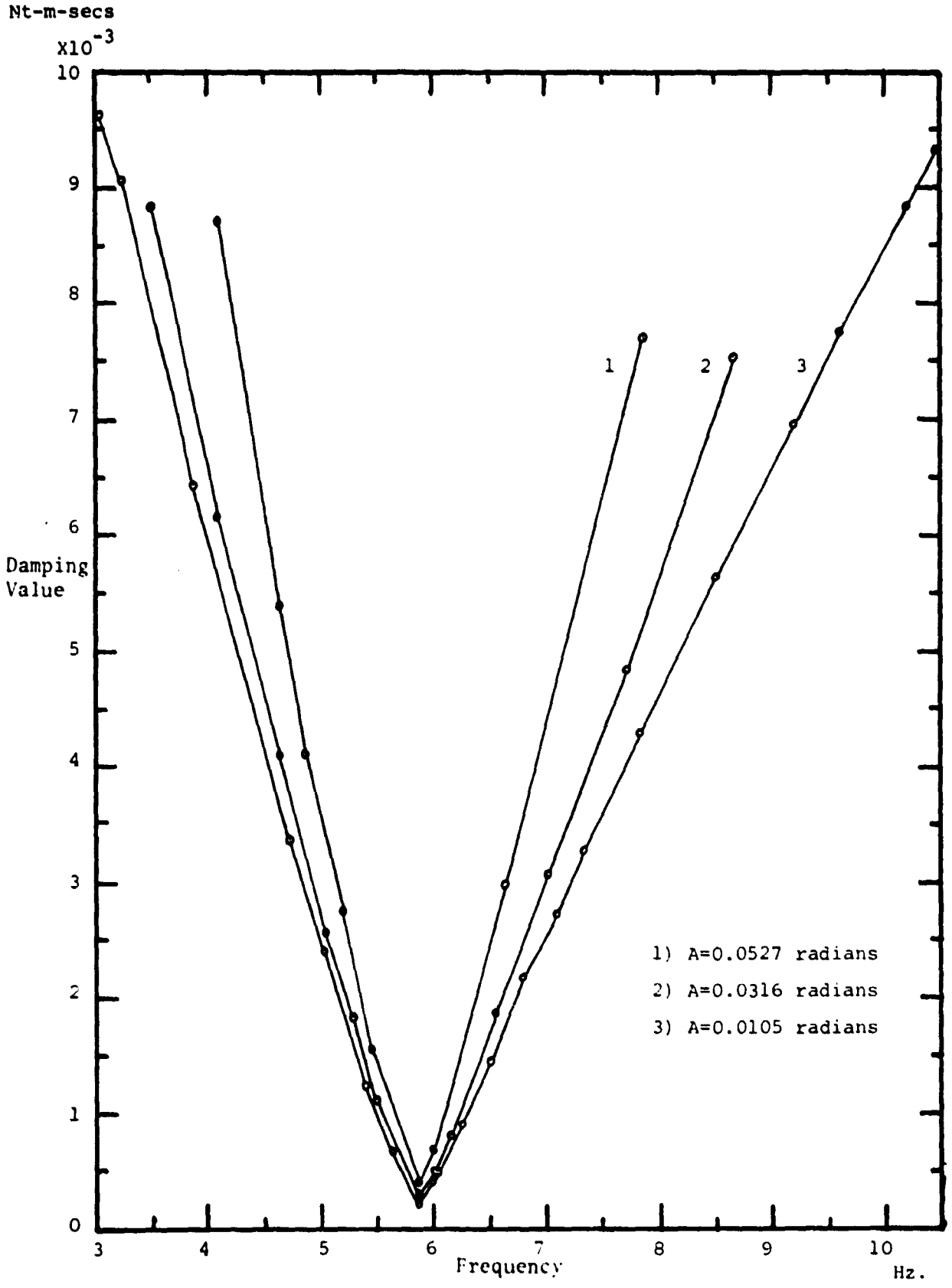

FIG. 9: Damping Value vs. Frequency for m_1=.0836 kg and l=.0545m

INTEGRATION OF ANALYTICAL RESULTS AND OPERATIONAL DYNAMICS

OPERATIONAL DYNAMIC MODEL

A damping mechanism causes a transfer of energy from one form to another. A force opposing velocity dissipates the kinetic energy while a force in the direction of velocity supplies energy thus exciting the motion. To control a structure (i.e., excitation or energy dissipation) the actuator reaction force must be proportional to the structure's velocity as illustrated in Eq. 14.

$$F_b = D\dot{x} \tag{14}$$

The amount of damping, or excitation, depends on the sign and magnitude of D. In order to excite a structure, to simulate a free-free assembly in an airless environment, D must be adjusted to provide as much energy to the structure as is dissipated through air drag, friction, etc.

In steady-state motion, the dynamic profile presented in the previous sections can be used to provide constant K and β values to generate an actuator response to an input if the desired frequency is known. But, to damp a transient response to an impulse, the superposition of mode shapes requires a breakdown of the motion to determine the required actuater frequencies and modal amplitudes. In the latter case, varying K and β values and numerous modal frequencies and shapes make exact control compensation difficult. By constructing a load cell mount for the actuater, a feedback loop can be used to compare desired and actual forces on the structure.

The actual dynamics of the actuator on a vibrating structure differs from the motion on the rigid mount used, in the previous sections, to find K and β. Fig. 10 shows the dynamic model of the PPM actuator during operation on a vibrating structure. Figs. 11a and b are force diagrams of the pivoting and

nonpivoting portions of the actuator.

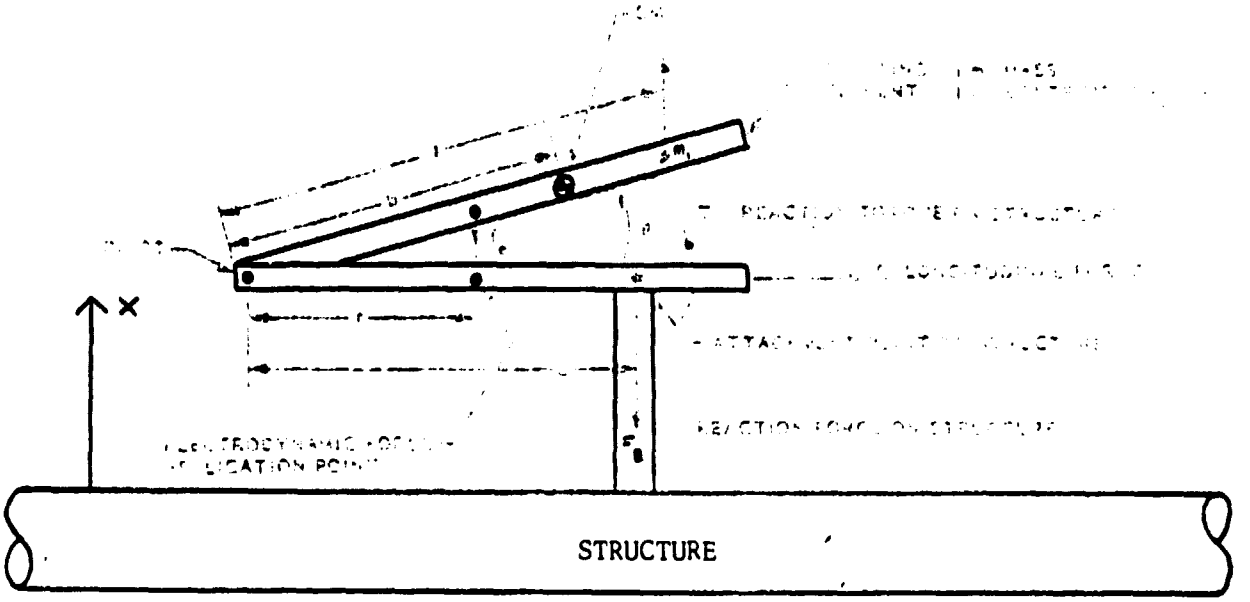

FIG.#10: PPM Actuator Operational Dynamics Model

Five components of torque, about the pivot, exist on the arm. Eq. 15 contains the rotational inertia, translational inertia, stiffness, damping and electromechanic torques (Refer to Fig. 11a). Summing the forces in the same figure, Eq. 16 is obtained. Summing the forces in Fig. 11b (Eq. 17) and combining with Eq. 16, Eq. 18 results. Eq. 18, along with Eq. 15, describes the dynamic response of the actuator during operation.

$$[I+mb^2]\ddot{\theta} + mb\ddot{x} + \beta\dot{\theta} + K\theta = f_e r \qquad (15)$$

$$F - f_e = m\ddot{y} = m[b\ddot{\theta} + \ddot{x}] \qquad (16)$$

$$F_b + F - f_e = m_2\ddot{x} \qquad (17)$$

$$F_b = (m_2 + m)\ddot{x} + mb\ddot{\theta} \qquad (18)$$

By knowing the desired force between the structure and actuator base, as

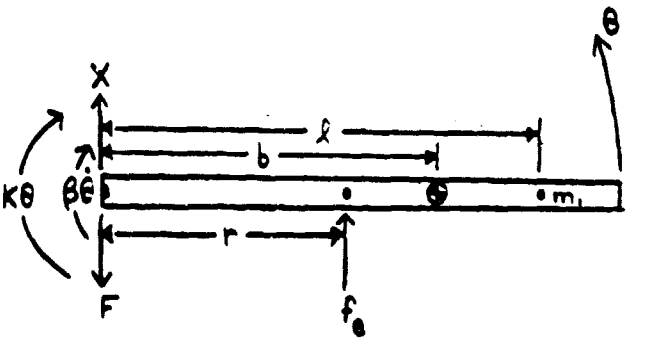

a) Pivoting Arm and Proof-Mass of Total Mass m

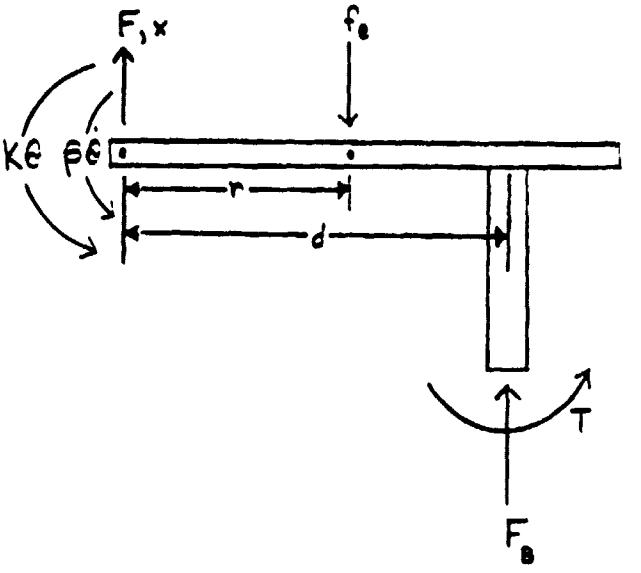

b) Nondivoting Mount of Mass m_2

FIG. 11: PPM Actuator Operational Force Diagrams

illustrated by Eq. 14, the proper f_e can be determined from Eqs. 15 and 18 through sensors and the dynamic coefficients. By substituting Eq. 18 into Eq. 15, one can determine the sensors required in the control system.

Summing the torques about the point of contact between the actuator and structure (Fig. 11b) one derives,

$$T = f_e r - md[b\ddot{\theta} + \ddot{x}]. \tag{19}$$

By combining Eq. 19 with the above equations, the torque can be found in terms

of the motion and eliminated by dimensioning (d) in Fig. 11b as described in Reference 1. The above results are verified through energy analysis and Lagrange's Equation.

STIFFNESS AND DAMPING APPROXIMATIONS

To simplify the control system, approximations of β and K should be used placing more responsibility on the feedback loop. An average value of K=0.42 N-m can be used and β can be read from Fig. 9 by shifting the frequency axis to align ω_n and the minimum point of the β curves (5.88 Hz.).

Once the approximate dynamic coefficients are chosen and incorporated into the control loop, the feedback mechanism will adjust the actuator f_e to the proper value based on the initial "guess". Assuming the motion of the structure is small, the K and β terms, determined using the original model, should provide reasonable accuracy when used with the operational dynamic model presented in the previous section.

ADDITIONAL ACTUATOR PROPERTIES

SPECIFICATIONS

Table 2 lists the various specifications describing the PPM actuator. Those values noted by an asterisk were provided by the Lockheed Missiles and Space Company but not verified in this analysis. The terms marked on the figures but not quantified in Table 2 (m_1, ℓ ,f_e,d) are variables that may be altered to provide the desired dynamic response. Eqs. 20a, b and c define the total mass of the pivoting arm, length from the pivot to the center of mass and inertia of the

TABLE 2: Prototype PPM Actuator Specifications

I_o	6.88×10^{-5}	kg-m^2	
m_o	0.088	kg *	
m_2	0.080	kg	
K_o	0.4506	Nt-m	at zero amplitude
K_{ave}	0.4200	Nt-m	
b_o	0.016	m *	
r	0.021	m *	
θ_m	0.067	radians *	
f_e	0.440	Nts/Volt	at 2.50 VDC polarization and zero deflection angle
Velocity Sensor	10.5	mv/rad/sec	

* indicates values not checked during this particular study.

arm about the pivot point.

$$m = m_o + m_1 \tag{20a}$$

$$b = [m_o b_o + m_1 \ell\ ]/m \tag{20b}$$

$$I+mb^2=I_o+m_1 \ell^2 \tag{20c}$$

MOTOR AND VELOCITY SENSOR CALLIBRATIONS

The electromagnetic moter was calibrated using the test setup shown in Fig. 5. A shim was placed between the load cell and proof-mass with the proper thickness to keep the arm at a zero deflection angle. Known input voltages were compared to output forces, multiplied by the ratio of the lever arms, to obtain 0.4352 Nts/volt$_{input}$ at 2.5 VDC polarization and zero deflection angle.

The velocity sensor, located at the end of the actuator opposite the proof-mass (Fig. 3), was analyzed to determine its effectiveness as one of the control loop sensors. Fig. 12 is a plot of the velocity sensor conversion factor (millivolts per radian per second) versus displacement amplitude. Above peak amplitudes of 0.002 radians, the conversion factor steadies. A slight dependency on frequency seems to exist but an average value of 10.5 mv/rad/sec was found as an asymptotic value for the curve in Fig. 12 for frequencies near resonance and amplitudes above 0.002 radians.

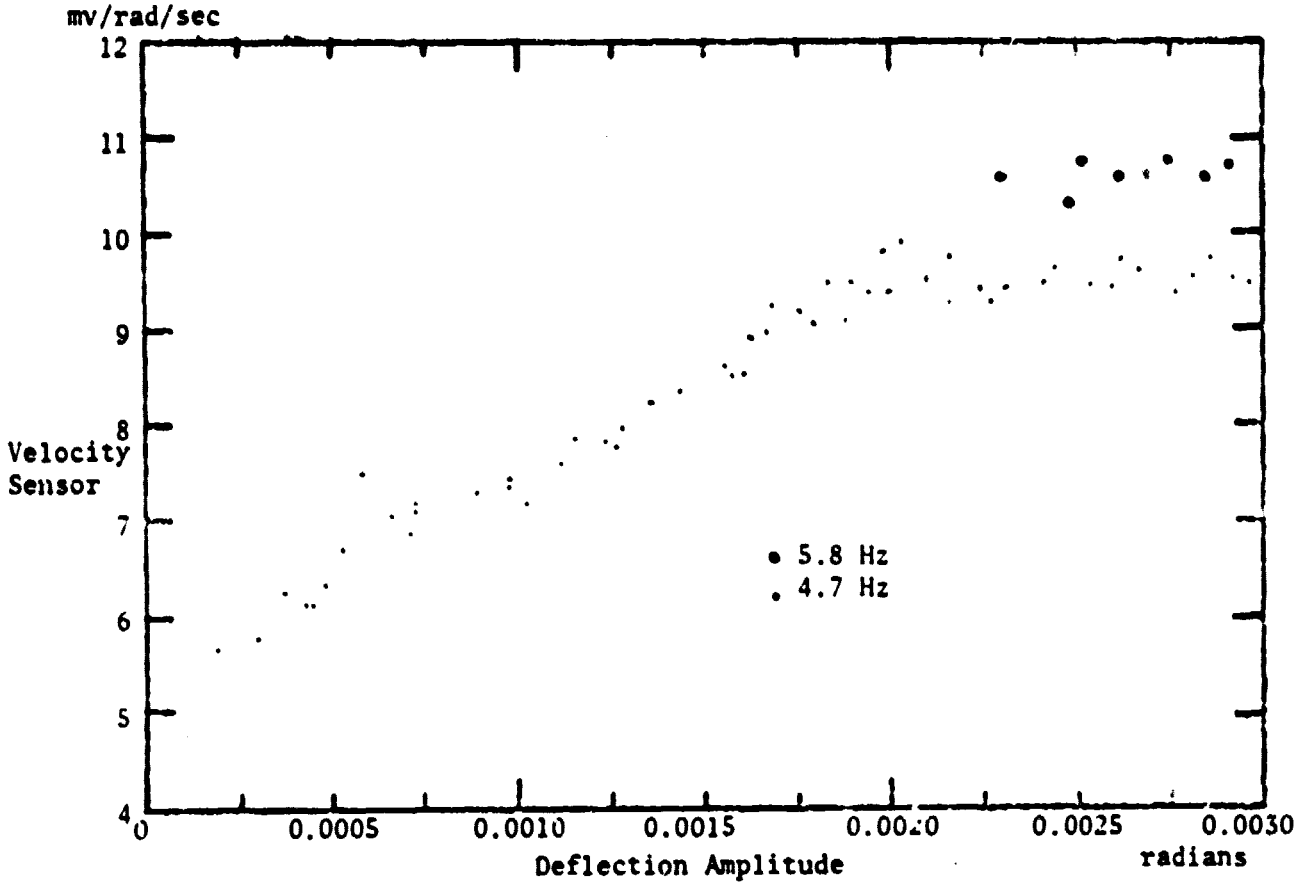

FIG. 12: Velocity Sensor Callibration vs. Deflection Amplitude for w_n = 6 Hz.

CONCLUSIONS AND RECOMMENDATIONS

Though nonlinearities exist in the actuator dynamics, convenient linear approximations are acceptable in a feedback control system. Throughout the arm deflection range, the stiffness value variation is minor and can be considered constant at the value given in the section on approximations. Although the damping value changes significantly throughout the actuator dynamic range, the pivoting arm is lightly damped and its value can be ignored in some control cases. Damping ratios range from about 0.002 at resonance to values much less than one tenth, far from resonance. Therefore, in damping a transient response, the approximations will be sufficient to provide effective feedback control.

The effectiveness of the prototype PPM Actuator declines significantly at frequencies less than 4 Hz due to the angular limit θ_m (Reference 1). An actuator can be sized for controlling lower frequencies but very low frequency control may be better performed by pivoting momentum wheels. The PPM Actuator is more appropriate as a higher frequency vibration controller as was evident in modal excitation tests performed on a pin-free beam.

One possible control loop can be devised by substituting for $\ddot{\theta}$ in Eq. 15, from Eq. 18, and using Eq. 14 to describe F_b. By using two accelerometers; one

$$(((mb)^2-[I+mb^2](m_2+m))/mbr)\ddot{x} + ([I+mb^2]D/mbr)\dot{x} + (\beta/r)\dot{\theta} + (K/r)\theta = f_e \qquad (21)$$

on the structure to be controlled and one on the proof-mass ; and subtracting and/or integrating the signals as necessary, the required input force f_e can be determined from the motion and the amount of damping D desired.

To aid in the control system, two types of feedback can be implemented.

Force feedback would compare the signal from a load cell mount, between the actuator and structure, to Eq 14. Secondly, a phase lock loop could be employed to drive the error signal; the phase between the structural velocity $\dot{x}$ and actuator force F_b; to zero. A knowledge of the dynamics of either or both feedback systems would be useful.

One detrimental feature of the PPM Actuator is a change, by some undetermined cause, from slight to critical damping. Periodically, this phenomenon would occur and may be a result of overheating in the actuator motor. Such an occurance significantly alters the dynamic response of the actuator and its cause should be investigated.

REFERENCES

1. J. N. Aubrun and G. Margulies, "Low-Authority Control Synthesis for Large Space Structures", NASA Contractor Report , Langley Research Center, May 1981.